International Journal of High Speed Electronics and Systems Vol. 32, Nos. 1 & 2 (2023) 2350004 (9 pages)

☐ World Scientific Publishing Company

□ World Scientific Publishing Company
DOI: 10.1142/S0129156423500040



Heating Effects on Nanofabricated Plasmonic Dimers with Interconnects

Rahul Raman, John Grasso and Brian G. Willis*

Chemical and Biomolecular Engineering, University of Connecticut, 191 Auditorium Road, Storrs, CT 06269, USA Brian.willis@uconn.edu

> Received 27 April 2023 Accepted 2 June 2023

Plasmonic nanostructures with electrical connections have potential applications as new electro-optic devices due to their strong light-matter interactions. Plasmonic dimers with nanogaps between adjacent nanostructures are especially good at enhancing local electromagnetic (EM) fields at resonance for improved performance. In this study, we use optical extinction measurements and high-resolution electron microscopy imaging to investigate the thermal stability of electrically interconnected plasmonic dimers and their optical and morphological properties. Experimental measurements and finite difference time domain (FDTD) simulations are combined to characterize temperature effects on the plasmonic properties of large arrays of Au nanostructures on glass substrates. Experiments show continuous blue shifts of extinction peaks for heating up to 210°C. Microscopy measurements reveal these peak shifts are due to morphological changes that shrink nanorods and increase nanogap distances. Simulations of the nanostructures before and after heating find good agreement with experiments. Results show that plasmonic properties are maintained after thermal processing, but peak shifts need to be considered for device design.

Keywords: Plasmonic dimers; nanofabrication; thermal annealing; localized surface plasmon resonance.

1. Introduction

Nanostructures made of materials such as Cu, Ag and Au may exhibit localized surface plasmon resonances (LSPR) that enhance interactions of light with matter [1, 2]. The spectral position of the resonances can be tuned by the size and shape of nanostructures so that they may act as tiny antenna to collect and concentrate electromagnetic (EM) radiation from the ultraviolet to the infrared. At resonance, EM fields are strongly enhanced around plasmonic nanostructures, and these fields may enable new types of electro-optic devices that convert radiation into electrical signals for applications as sensors or for solar energy harvesting. For example, LSPR-generated EM fields may stimulate production of hot carriers that traverse Schottky barriers to create photocurrents for light sensors [3]. EM field enhancements are known to be especially strong at sharp tips and in nanogaps formed

^{*} Corresponding author

between closely spaced particles. When nanogaps are formed between sharp tips, EM field enhancements can exceed 10³ [4]. Achieving such strong field enhancements may be critical for creating efficient devices.

The vast majority of studies related to plasmonics have investigated nanoparticles suspended in solution or randomly dispersed on solid supports. However, when ordered structures are created by nanofabrication techniques, it is possible to add electrical interconnections to plasmonic nanorods for electro-optic functions [5]. Nanofabrication, thin film deposition, and reactive processes provide opportunities for engineering plasmonic nanostructures to tune their optical properties and create nanogaps for enhanced EM fields. For example, atomic layer deposition (ALD) can be used to tune nanogap sizes and integrate plasmonic nanostructures with other materials [6].

In general, nanofabrication and thin film engineering to create functional devices will require thermal processes. In some cases, thermal processing may exceed temperatures of 200°C. These thermal treatments may affect plasmonic properties and need to be factored into device design. Previous research on ALD-processed plasmonic nanostructures found significant blue shifts after thermal processing that were unexpected based on uniform and conformal growth [6]. In this study, we investigate optical and morphological changes of nanostructures after thermal treatments to determine how temperature affects plasmonic properties. As a model system, we investigate nanostructures made of Au on clear glass substrates. Optical extinction curves are measured before and after thermal treatments at temperatures up to 210°C to determine how heating affects plasmonic properties. We also investigate structural changes using high-resolution electron microscopy.

2. Experiment

Nanostructures were fabricated as large arrays of interconnected nanorod dimers using electron beam lithography with a F125 electron beam writer (Elionix, Japan), and using poly(methyl methacrylate) (PMMA) photoresist (Kayak, USA). The design uses a 550 nm square unit cell repeated over an array 200 x 200 um² square. Substrates were 75 mm diameter fused silica wafers (GM Glass, USA). E-spacer was used for charge dissipation (Showa Denko, Japan). After development with methyl isobutyl ketone and isopropyl alcohol (MIBK/IPA), samples were rinsed with IPA, dried with N₂ gas and processed with a 75 W O_2 plasma in a barrel etcher before metal deposition. A thin film stack of 4 ± 1 nm Ti and 45 ± 5 nm Au was deposited in a high vacuum electron beam evaporator (Denton Vacuum, USA). Samples were further processed by liftoff using Remover PG (Kayak) to reveal the nanostructure arrays. A second layer of photolithographic processing was used to add electrical connections and guide marks for optical beam alignment. The second layer used a Shipley resist s1805 (Shipley, USA), and an MLA-150 lithography tool (Heidelberg, Germany). Metal deposition was done in the same electron beam evaporation tool using Ti/Au layers of 10/200 nm, respectively. Liftoff used the same procedures as the first level. After liftoff, samples were rinsed with IPA and dried with N2 gas before optical measurements.

Samples were heated in air on a hot plate at atmospheric pressure with a range of temperature setpoints for 20 minutes. A thermocouple was used to calibrate sample temperatures by attaching it to a blank substrate with similar properties as the samples with nanofabricated devices. Samples were cooled in air for 10 minutes before being mounted to an ellipsometer for optical measurements.

Optical extinction measurements were taken with a JA Woollam M2000V spectroscopic ellipsometer operating in transmission mode. Reference transmission spectra were taken adjacent to feature arrays, and extinction was calculated as $(1-T/T_R)$, where T_R is the reference transmission of clear glass. The optical beam is approximately 200 um in diameter and collects data from more than 10^5 nanostructures in each array. Secondary electron microscopy (SEM) images of samples before and after heating were taken with a high-resolution Verios SEM (ThermoFisher Scientific). A thin (few nm) layer of AuPd was sputtered onto samples for charge dissipation. SEM images of before-heating samples were taken from an adjacent die, whereas post-SEM images are from the same die used for optical data before and after heating. SEM images were analyzed using PROSEM software (GeniSys, Germany) to calculate average nanostructure sizes and interparticle distances. The reported data are averages of 20 different feature measurements.

Simulations of optical extinction spectra used finite difference time domain (FDTD) methods as implemented in Lumerical commercial software (Ansys, USA). Geometric structures were extracted from high-resolution images recorded with the Verios SEM. Representative structures were extracted from images and used in the FDTD simulations. Two-dimensional (2D) images were converted to 3D shapes by extruding the image outlines along the z-direction a distance corresponding to the thin film thickness. This procedure gives a flat profile for the tops of simulated features. The model nanostructures were placed on a SiO₂ substrate and transmission spectra were calculated. Periodic boundary conditions were applied to the horizontal boundaries of the 3D simulation cell, and a plane wave polarized along the length direction of the nanorods was directed towards the nanostructures in the vertical direction. The same unit cell size of 550 nm square was used for experiments and simulations. Optical constants were taken from the Lumerical library using data from Palik for Ti and SiO₂, and Johnson and Christy for Au [7, 8].

3. Results and Discussion

Figure 1 shows a schematic of the design for interconnected plasmonic dimers, which consist of nanorod dimers with interconnect lines running through the centers of the nanorods. The interconnect lines are 45–50 nm in width, which is close to the resolution limit of the nanolithography methods used. The center positions of the interconnect connections are chosen based on prior work that determined center contacts provide the least perturbation to nanorod plasmonic resonances [9, 10]. The configuration of nanorod dimer pairs with small nanogaps promotes strongly enhanced EM fields in the regions between the tips of the nanorods [11]. Electrical interconnects allow for future

4 Raman, R., Grasso, J., Willis, B.G.

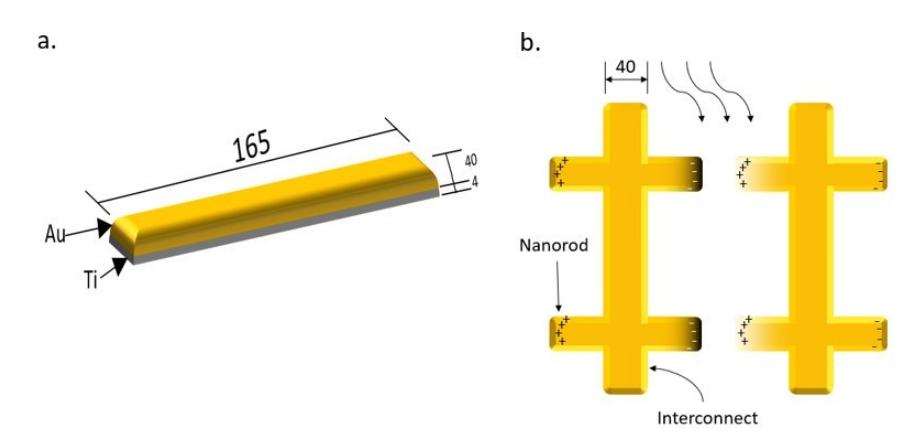


Fig. 1. Nanorods are paired to form plasmonic dimers with interconnects. Dimensions are given in nm. (a) Side view of nanorods. (b) Top view of nanorods with interconnects.

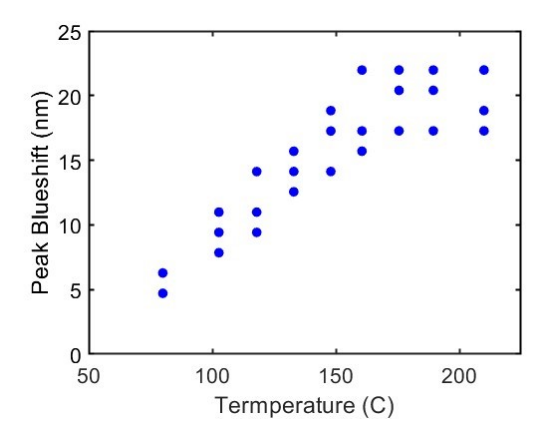


Fig. 2. Blue shifts of peak wavelengths relative to spectra taken before heating are shown vs. temperature.

applications of voltages and measurements of photocurrents while exciting plasmon resonances with light.

Optical extinction spectra were investigated using a series of thermal treatments up to 210°C with incremental heating starting from 80°C. Heating causes blue shifts of the extinction peaks that increase with temperature, but no significant changes of extinction magnitudes were observed. A plot of blue shift vs. temperature is shown in Fig. 2. The data are scattered, but the trend shows a linear increase of blue shifts with temperatures that exceed 20 nm at the maximum temperature of 210°C. The maximum temperature of the experiments was limited by the hot plate specifications, but the effect does not saturate, and higher temperatures may lead to even larger blue shifts. The shifts of the extinction spectra indicate some changes in the optical or morphological properties of the nanostructures. High-resolution electron microscopy and FDTD simulations were used to further investigate the blue shifts.

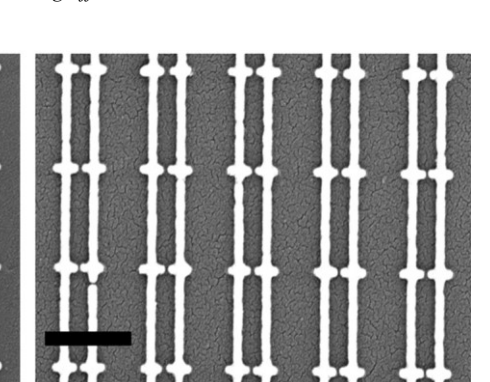


Fig. 3. SEM images from different stages of heating. (Left) Before heating. (Right) After heating to 210°C. Scale bar is 500 nm.

High-resolution electron microscopy was used to investigate morphological changes of the nanostructures and to extract nanostructure shapes for FDTD modeling. Figure 3 shows example SEM images before and after heating for a sample heated to the maximum temperature of 210°C. The microscopy studies reveal significant heat-induced changes of the nanostructures, including shrinking along length directions and increases in width directions. Shrinking of dimer pairs in length also causes increases of nanogap distances between nanorods. The increased interparticle distances due to nanorod shrinking are a significant factor in the blue shifts. Previous studies of nanoparticle dimers have shown that resonance peak wavelengths are highly sensitive to interparticle distances with an exponential dependence for very small nanogaps [12].

Measurements of nanostructures before and after heating show significant morphological changes. Before heating, average nanorod lengths and widths were 161.5 ± 5.5 nm and 50.5 ± 0.5 nm, respectively. Interparticle separation was 16 ± 5 nm. After heating to the maximum temperature of 210° C, the average length shrinks to 154.5 ± 7 nm, and the width increases to 55.5 ± 1 nm. The change of length is -7 nm, which is slightly larger than the width increase of +5 nm. The shrinking and broadening of the nanostructures cause nanogap distances to increase by 5.5 nm to 21.5 ± 4 nm. The magnitudes of the nanogap increases are roughly consistent with the magnitudes for length contractions. The morphological changes are consistent with thermodynamic driving forces to minimize surface area and round sharp corners toward more spheroidal shapes. Although temperatures are far below the melting point of Au (1064° C), the small sizes and large surface to volume ratios of the nanorods may promote rapid surface diffusion and mass transport driven by surface energy reduction. Other studies of Au nanorods have also reported the tendency for Au nanorods to spheroidize at temperatures higher than 80° C [13].

FDTD simulations were investigated to connect morphological features with optical properties. Optical extinction data taken before and after heating to the highest temperature of 210°C are shown in Fig. 4, along with FDTD simulations. The simulations use

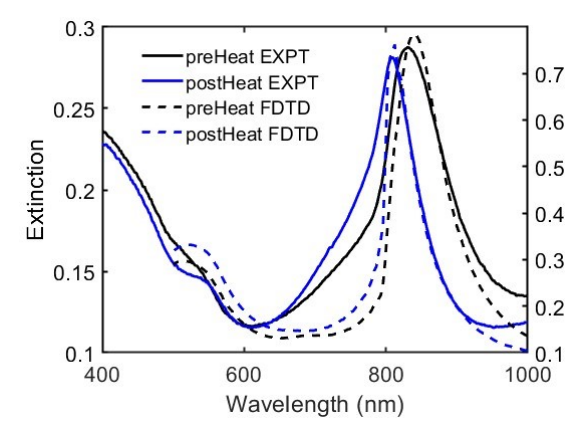


Fig. 4. Experimental (solid) and FDTD (dashed) extinction spectra before and after heating to 210°C. The left axis is for experiments and the right is for FDTD simulations.

representative geometric structures extracted from the experimental SEM images in Fig. 3. Experimental spectra for before-heating measurements have an extinction peak at 831 nm, while FDTD simulations peak at 840 nm. The thickness modeled is Ti/Au 4/50 nm, which is within the expected range for experimental thickness. The peak locations are very close, but could be closer by using a thicker Au layer in the simulations, which would blue shift the resonance a small amount. A slightly larger nanogap would also blue shift the resonance. Deviations of experiments from a flat top surface could also account for some of the difference.

Full-widths at half-maximum (FWHM) were extracted from experiment and simulation curves by fitting the peak maxima and high wavelength leading edges to Lorentzian line shapes. This partial peak fitting was used to avoid the influence of diffraction effects that distort the blue side of the extinction peaks. The diffraction effect occurs near 800 nm due to the coincidence of the SiO₂ index of refraction (1.45) and the periodicity of the lattice at 550 nm. Using this approach, before-heating experiments have FWHM of 100, while FDTD simulations are 90 nm. These values are larger than what is obtained for a full peak fit due to the diffraction effects. The larger peak width for experiments is expected due to inhomogeneous broadening from variations of the nanorod sizes across the large arrays. Electron-beam lithography proximity error may account for ± 5 nm peak wavelength variation across the 200 x 200 um² array. A Ti adhesion layer used in experiments was included in the FDTD model. Simulations show that Ti layer thickness strongly affects the FDTD curve FWHM, and a thicker layer would broaden the peaks and bring simulations closer to experiments. The FWHM of the before-heating experiments and FDTD simulations are remarkably close considering that the experiments are sampling $> 10^5$ structures, while simulations are only modeling a single representative structure extracted

from SEM images. Considering the large number of nanostructures sampled by the optical bream, the overall agreement between experiment and theory is very good.

After heating, nanorods shrink in length and expand in width, while nanogaps increase. These changes are expected to blue shift the resonances, and experiments bear this out. After heating, experimental spectra blue shift by 23 nm to 808 nm. FDTD simulations using structures extracted from post-heating SEM images in Fig. 3 show a similar blue shift of 28 nm to 812 nm. The leading edges of the two plots overlap significantly, and the (partial fit) FWHM are similar, with experiment at 81 and FDTD simulation at 86 nm. The smaller FWHM for experiment is an artefact of the peak fitting range, and a full fit to the FDTD curve gives FWHM close to 52 nm, but the peak shape is distorted by the diffraction effect. The diffraction effect is not as apparent in the experiments due to the irregular nature of the scatters and the finite size of the lattice. However, both pre- and post-heating experimental curves show a shoulder on the blue side of the peak that may be due to a partial influence of the diffraction effect. This effect may also account for the broad tail between 700 and 800 nm in the experimental spectra. Interestingly, the experimental post heating spectra have a narrower FWHM than the before-heating spectra, which is predicted by the simulations. The narrowing of the experimental peak further indicates that a diffraction effect may be influencing the spectra. The close match of experiments and simulations is evidence that the optical properties (refractive index) of the Au nanorods are not changed by heating in air. This is unlikely to be the case for Cu or Ag materials where extensive oxidation may occur without an inert atmosphere. The good agreement also suggests that the Ti adhesion layer at the SiO₂ interface is reasonably well modeled as a metallic layer.

Besides the main LSPR peak, experiments and simulations show a second feature near 530 nm that is assigned to the transversal resonance of the interconnect lines that run through the centers of the nanorods. This second peak is not seen for plasmonic dimers without interconnects. The experimental peaks are partly obscured by a rising background below 500 nm, but the features are clearer in spectra from different samples. The peak locations are similar for experiments and simulations. Baseline extinction levels away from the peaks are also similar for experiments and simulations, with an extinction level near 0.1. In contrast, extinction peak maxima are more than a factor of two different experiments. The discrepancy of extinction maxima is partly due to inhomogeneous broadening from size variation across the large arrays. Another factor is the difference between the optical properties of nanostructures vs. the bulk optical constants used for simulations. Both experiments and simulations show a slight reduction of maximum extinction levels after heating but the difference is small.

We also investigated the effects of the Ti adhesion layer on the optical properties of plasmonic nanostructures using FDTD simulations. Experimentally, a thin layer of Ti is necessary to promote adhesion between Au nanostructures and SiO₂ (quartz) substrates. The Ti layer is known to dampen plasmon resonances, but direct Au/SiO₂ interfaces are unlikely to survive nanofabrication processes such as liftoff, where aggressive chemicals and ultrasonic agitation are used. Figure 5 shows a comparison of FDTD simulations with and without a 4 nm Ti layer between Au and SiO₂. Peak wavelengths are similar for post-

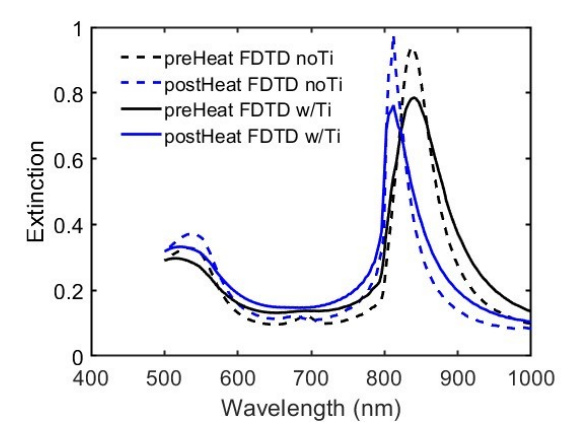


Fig. 5. Comparison of FDTD simulations before heating (black) and after heating (blue) with and without a 4 nm Ti layer.

heating extinction curves, but pre-heating data without Ti are slightly shifted to the blue at 836 nm compared to 840 nm with Ti. As expected, FWHM are larger for simulations with Ti. For partial peak fitting in the region 700-1000 nm, FWHM calculated before heating increases from 55 to 80 nm when Ti is added. For post-heating simulations, the increase is from 33 to 52. These values are dependent on the peak fitting region, but qualitatively, they show that Ti layers significantly broaden extinction curves. Including a Ti layer also decreases peak heights. For pre-heating plots, the peak is 16% smaller than for pure Au. After heating, simulations without Ti predict an increased extinction level, whereas peak extinction decreases when Ti is considered. Minimizing Ti layer thickness without losing device yield may enhance optical properties and device performance.

4. Conclusion

Heating nanofabricated Au plasmonic dimers with interconnects shows changes of optical extinction spectra that blue shift with increasing temperatures. High-resolution electron microscopy imaging shows that heating causes shape changes that reduce lengths and increase widths of nanorods, while increasing the distances between nanostructures. FDTD simulations using nanostructures extracted from images with and without heating show good agreement with experiments, which indicates that the morphological changes are the cause of the blue shifts. Peak widths are broader for experiments due to inhomogeneous broadening, but the differences are small when considering the large number of nanostructures sampled in the optical beam. The arrays provide strong plasmonic resonances that can be improved further by optimizing uniformity and reducing the thickness of the Ti adhesion layer. Heating causes blue shifts, but peak intensity and width are not significantly affected. Thermal processing induces blue shifts that need to be accounted for in device design, but these studies show that plasmonic resonances are not degraded.

Acknowledgments

The authors acknowledge the National Science Foundation (NSF) (Grant No. 2150158) and the Office of Naval Research (Grant No. N00014-22-1-2567). This work was performed in part at the Harvard University Center for Nanoscale Systems (CNS); a member of the National Nanotechnology Coordinated Infrastructure Network (NNCI), which is supported by the National Science Foundation under NSF award no. ECCS-2025158.

Electron microscopy was performed at the UConn/Thermo Fisher Scientific Center for Advanced Microscopy and Materials Analysis (CAMMA).

References

- 1. E. Ozbay, Science **311** (5758), 189-193 (2006).
- 2. S. A. Maier, Plasmonics: Fundamentals and Applications (Springer, New York, 2007).
- M. W. Knight, H. Sobhani, P. Nordlander and N. J. Halas, Science 332 (6030), 702-704 (2011).
- 4. D. R. Ward, F. Huser, F. Pauly, J. C. Cuevas and D. Natelson, Nature Nanotechnology 5 (10), 732-736 (2010).
- 5. P. Pertsch, R. Kullock, V. Gabriel, L. Zurak, M. Emmerling and B. Hecht, Nano Letters **22** (17), 6982-6987 (2022).
- 6. C. Zhang, T. Gao, D. Sheets, J. N. Hancock, J. Tresback and B. Willis, Journal of Vacuum Science & Technology B **39** (5), 053203 (2021).
- 7. E. D. Palik and G. Ghosh, *Handbook of Optical Constants of Solids*, ed. Edward D. Palik. (Academic Press, Orlando, 1985).
 - P. B. Johnson and R. W. Christy, Physical Review B 6 (12), 4370-4379 (1972).
- 8. J. C. Prangsma, J. Kern, A. G. Knapp, S. Grossmann, M. Emmerling, M. Kamp and B. Hecht, Nano Letters 12 (8), 3915-3919 (2012).
- 9. D. T. Zimmerman, B. D. Borst, C. J. Carrick, J. M. Lent, R. A. Wambold, G. J. Weisel and B. G. Willis, Journal of Applied Physics **123**, 063101 (2018).
- P. Nordlander, C. Oubre, E. Prodan, K. Li and M. I. Stockman, Nano Letters 4 (5), 899-903 (2004).
- 11. C. Tabor, R. Murali, M. Mahmoud and M. A. El-Sayed, The Journal of Physical Chemistry A **113** (10), 1946-1953 (2009).
- 12. S. S. E. Collins, M. Cittadini, C. Pecharromán, A. Martucci and P. Mulvaney, ACS Nano 9 (8), 7846-7856 (2015).